Int. J. Heat Mass Transfer. Vol. 35, No. 9, pp. 2173–2183, 1992
Printed in Great Britain

0017–9310/92 $5.00 + 0.00

Flow and heat transfer to a circular cylinder with a hot impinging air jet

S. H. KANG† and R. GREIF
Department of Mechanical Engineering, University of California at Berkeley, Berkeley, CA 94720, U.S.A.

(*Received* 9 *July* 1991 *and in final form* 30 *August* 1991)

Abstract—A study has been made of the flow and heat transfer to a circular cylinder from a hot impinging air jet. The problem is of fundamental interest and also has important applications; e.g. in respect to the outside vapor deposition process. Numerical solutions of the governing conservation equations have been obtained utilizing a non-orthogonal curvilinear coordinate grid. The effects of the Reynolds and Grashof numbers on the flow and heat transfer, as well as those of the wall temperature, the jet width, and the distance between the nozzle and the cylinder have beeen investigated and correlation curves are presented. The flow is stable and symmetric over the range of parameters studied. The interaction of the buoyant impinging jet with the cylinder as well as with the surroundings makes the flow and heat transfer to the cylinder quite different from that for uniform flow. The effects of buoyancy, diffusion and cooling of the jet ahead of the cylinder, the development of the wall jet, and the recirculating bubble all affect the flow and heat transfer. The average Nusselt number increases with increasing Reynolds and Grashof numbers and narrow banded correlation curves are obtained by introducing an effective Reynolds number, which includes a buoyancy contribution. The width of the jet and the distance between the nozzle and the cylinder have a strong effect on the heat transfer.

1. INTRODUCTION

THE MANUFACTURE of high quality wave guides has been successfully carried out utilizing particle deposition techniques. Three vapor deposition processes have been widely used to manufacture the optical fiber preforms; namely, modified chemical vapor deposition (MCVD), outside vapor deposition (OVD) and vapor phase axial deposition (VAD). In the OVD process, the torch is composed of concentric rings through which $SiCl_4$, CH_4, O_2, and N_2 gases flow. The torch traverses and heats the surface of a horizontal cylindrical target. As the $SiCl_4/O_2$ stream reacts in the presence of either hydrogen or methane, silica particles are formed by direct oxidation or hydrolysis reactions. Silica particles deposit on the cylinder due to thermophoresis. In the manufacture of the preform, the silica deposition rate on the target is an essential factor in the efficiency of the process. The complex effects resulting from the torch flow and heat transfer, combustion, silica particle formation and deposition etc., make control and optimization of the OVD process considerably difficult. Homsy *et al.* [1] and Batchelor and Shen [2] analysed the thermophoretic deposition of particles in a uniform flow past a cylinder based on the Blasius series solution. Garg and Jayaraj [3, 4] calculated thermophoretic deposition over a cylinder in numerical studies specifying the pressure gradient of the external flow. Alam *et al.* [5] have investigated the thermophoretic deposition associated with a plane jet impinging on a flat plate. These studies have utilized boundary layer assumptions with simple external flows. However, experimental results [6, 7] have shown that the circumferential variation of the flow and heat transfer, as well as the interaction between the torch and the boule, have strong effects on the particle deposition. Accordingly, it is anticipated that an analysis of the phenomena utilizing the governing elliptic conservation equations is appropriate and in this work a study has been made of a buoyant jet impinging on a circular cylinder.

Studies have previously been carried out for an external uniform flow past a horizontal circular cylinder. A review of the heat transfer from tubes in a cross flow has been reported by Zukauskas [8]. Mixed convection transport from a horizontal cylinder has been summarized by Morgan [9] and by Gebhart *et al.* [10]. The average heat transfer from cylinders in the various flow regimes is given as a function of the Reynolds and Grashof numbers. It is noted that the flow and temperature fields for a buoyant impinging jet are quite different from the results for a uniform flow.

When a hot air jet impinges on a circular cylinder, the flow around the cylinder can be divided into the following regions: (a) free jet, (b) stagnation, (c) wall jet, (d) near wake recirculation, and (e) buoyant far jet-wake regions. As the air leaves the nozzle, which is located sufficiently below the cylinder, a free buoyant jet is assumed to develop from a potential core region. The plane buoyant jet may be considered to be laminar when its Reynolds number, based on the

† Visiting Professor from Seoul National University, Seoul 151-742, Korea.

NOMENCLATURE

A_i	convection–diffusion coefficients
a^i	contravariant base vector
b	source term in the discretized equation
C_f	skin-friction coefficient $[= 2\tau/\rho U_j^2]$
C_p	pressure coefficient $[= 2p/\rho U_j^2]$
c_p	specific heat at constant pressure
Gr	Grashof number $[= g\beta R^3(T_j - T_a)/\nu^2]$
g	square of the Jacobian
g_v	gravitational acceleration
g^{ij}	components of the contravariant metric tensor
H	distance between the nozzle and the cylinder
h	heat transfer coefficient $[= q/(T_j - T_a)]$
i, **j**	Cartesian base vectors
k	conductivity
L_s	separation length
Nu	Nusselt number $[= hR/k]$
Pr	Prandtl number $[= \mu c_p/k]$
p	static pressure
R	radius of a cylinder
Re	Reynolds number $[= U_j R/\nu]$
S_ϕ	source term in the governing equation
T	temperature
U^i	contravariant velocity component
U_j	magnitude of the jet velocity
u, v	Cartesian components of the velocity
W	half width of the jet
x, y	Cartesian coordinate.

Greek symbols

β	expansion coefficient of the air
Γ	general diffusive coefficient
Δ	non-dimensional wall temperature $[= (T_w - T_a)/(T_j - T_a)]$
θ	angle measured from the front stagnation point
μ	viscosity
ν	kinetic viscosity
ξ^i	curvilinear coordinate $[\xi^1 = \xi, \xi^2 = \eta]$
ρ	density
τ	wall shear stress
ϕ	general dependent variable.

Subscripts

a	ambient value
eff	effective value defined in equation (11)
j	jet value
N, S, E, W	four nodes around the grid point P
w	wall value
ξ^i	partial differential operator w.r.t. ξ^i.

radius of the cylinder and the jet velocity, is less than 1000; the transition Reynolds number is reported to be between 1000 and 3000, and varies with the jet width and the exit velocity [11]. As the jet approaches the cylinder there is a rapid increase in the static pressure; for a jet impinging on a flat plate this occurs at about one quarter of the distance between the plate and the nozzle exit [12]. For the cylinder, this location is shown to depend strongly on the radius of the cylinder. Beyond the stagnation point the flow accelerates and develops into a wall jet which may separate downstream. If there is no vortex shedding, the flow will be steady. For steady flow, a recirculation bubble will form at the rear of the cylinder and further downstream a buoyant jet will develop. In the present study the flow is assumed to remain laminar throughout the entire domain. For a hot jet there will be a strong buoyancy force acting vertically as well as lateral diffusion and cooling. From the stagnation point to the recirculation region, the hot gas will continue to heat the cylinder and be affected by buoyancy. The jet will also lose some energy to the ambient air. Results for the flow and heat transfer are presented for a range of values of the dimensionless parameters.

2. MATHEMATICAL MODELING

2.1. *Coordinates and governing equations*

The flow is assumed to be laminar and steady and the fluid properties are considered to be constant except for the buoyant density term, which is given by the Boussinesq approximation. The governing equations are described in the Cartesian coordinate system where u and v denote velocity components in the x- and y-directions, respectively (cf. Fig. 1). A non-orthogonal curvilinear coordinate grid is generated to carry out the numerical calculations [13–15]. Since the local heat transfer on the surface of the cylinder, especially near the stagnation point, is of interest, the so called C-type grid system is adopted [13], which

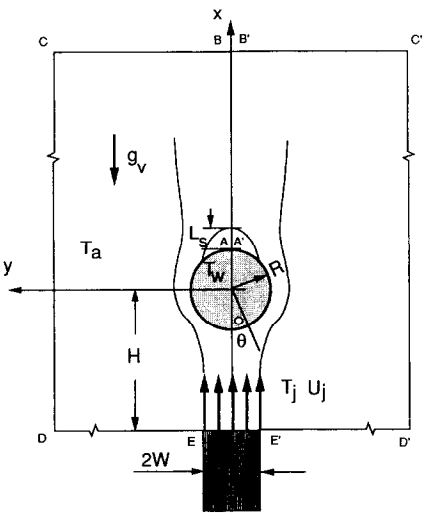

FIG. 1. Flow configuration and coordinate system.

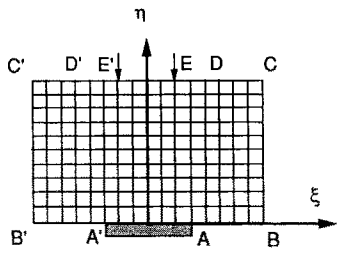

FIG. 2. Transformed domain for numerical calculations.

smoothly aligns the grids in this region. The center line of the wake ($x > 1.0$, $y = 0.0$) is a branch-cut which transforms the flow domain to a rectangular region, as shown in Fig. 2. The transformation functions $\xi(x, y)$ and $\eta(x, y)$ are obtained by solving Poisson equations [14, 15].

The governing equations written in conservative form relative to an arbitrary curvilinear coordinate system are as follows:

continuity equation,

$$(\sqrt{g}\rho U^i)_{\xi^i} = 0 \tag{1}$$

x-momentum equation,

$$[\sqrt{g}(\rho U^i u - \mu g^{ij} u_{\xi^j})]_{\xi^i} + (y_{\xi^2} p)_{\xi^1} - (y_{\xi^1} p)_{\xi^2} - \sqrt{g}\rho g_x \beta (T - T_a) = 0 \tag{2}$$

y-momentum equation,

$$[\sqrt{g}(\rho U^i v - \mu g^{ij} v_{\xi^j})]_{\xi^i} + (x_{\xi^2} p)_{\xi^1} - (x_{\xi^1} p)_{\xi^2} = 0 \tag{3}$$

energy equation,

$$[\sqrt{g}(\rho c_p U^i T - k g^{ij} T_{\xi^j})]_{\xi^i} = 0 \tag{4}$$

where

$$\xi^1 = \xi, \quad \xi^2 = \eta, \quad U^i = \vec{a}^i \cdot (u\hat{i} + v\hat{j}),$$
$$\vec{a}^i = \nabla \xi^i, \quad g^{ij} = \vec{a}^i \cdot \vec{a}^j. \tag{5}$$

2.2. *Boundary conditions*

The no-slip condition for the velocity components and the condition of constant wall temperature are given on A′–A, which is the transformed circular cylinder. The results should be symmetric about $\xi = 0$, but the symmetry condition is not invoked. The velocities and temperature along A–B are equal to those along A′–B′. Note that vortex shedding and asymmetric configurations would result in asymmetry and unsteadiness which are not studied in the present work. On E′–E, corresponding to the nozzle exit, the velocity and temperature are uniform, i.e. $u = U_j$, $v = 0$, and $T = T_j$. The static pressure is fixed to be zero here as a reference value. On the boundaries C′–D′ and D–C, which are located far from the cylinder, the y derivative of the entrained horizontal velocity component is taken to be zero:

$$\frac{\partial v}{\partial y} = 0. \tag{6}$$

The boundary condition for u is determined by considering the entrained flow to be irrotational:

$$\frac{\partial^2 u}{\partial y^2} = 0. \tag{7}$$

The entrained flow is assumed to be horizontal at the external upstream boundary: D–E and E′–D′. This assumption does not have a strong effect on the flow pattern and heat transfer over the cylinder. The temperature on the external boundary is at the constant ambient value:

$$T = T_a. \tag{8}$$

At the far downstream location above the cylinder, B′–C′ and B–C, the streamwise second derivatives of the velocity components and the temperature are assumed to be zero.

3. NUMERICAL METHOD

The governing equations (1)–(4) can be written in a generalized form according to

$$[\sqrt{g}(\rho U^i \phi - \Gamma g^{ij} \phi_{\xi^j})]_{\xi^i} - b = 0 \tag{9}$$

where ϕ denotes an arbitrary variable, thus admitting a common solution procedure. All the dependent variables are calculated and stored at the same intersection of grid lines rather than at the staggered grid locations. The discretized form of the equations is obtained by the finite volume method (cf. Patankar [16]) and is written as

$$A_P \phi_P = A_N \phi_N + A_S \phi_S + A_E \phi_E + A_W \phi_W + S_\phi. \tag{10}$$

The coefficients A_i are obtained by integrating the convective and diffusive fluxes across the control surfaces and the subscripts N, S, E, and W denote the four neighboring grid points around P. Since the Reynolds numbers are not large, the HYBRID scheme is used [16]. The quantity S_ϕ includes all the terms proportional to the control volume and related to the non-orthogonal coordinate grid.

The calculation of the pressure proceeds according to the SIMPLE algorithm of Patankar [16] by making corrections at each iteration, until the velocities and the corrected pressure field satisfy the continuity and momentum equations. To avoid oscillating results in the non-staggered grid system, linearized solutions of the momentum equation are used at each control surface to evaluate the fluxes. These are obtained by using the velocities and pressures at neighboring points [14, 15].

A Modified Strongly Implicit (MSI) method [17] is adopted to solve the discretized linear equations. The method gives fast convergence and is relatively insensitive to the control volume aspect ratio. Velocities are calculated with assumed velocity, pressure and temperature fields. Then the pressure at each node is corrected and the temperature field is calculated. The overall solution is iterative in nature and convergence is checked by monitoring the sum of the residuals

for the variables over the entire domain. The code was developed from a code provided by Professor Humphrey which is reported in Schuh *et al.* [15]. The numerical method and performance of the code were first studied for natural convection in a square cavity and for forced convection past a cylinder. The former problem is that of steady, buoyant flow in a square enclosure with vertical sides which are differentially heated and horizontal surfaces which are insulated [18]. The flow and Nusselt number distributions were in excellent agreement with the published results.

The flow and heat transfer around a circular cylinder in a uniform hot air stream have also been determined. For this test case, calculations were carried out for $Re = 20$. After several calculations were made with different locations of the boundaries and mesh numbers, the upstream and downstream locations were chosen to be $-1.0H$ and $20.0R$, and the external boundaries were located at $\pm 10.0R$. The number of grid points was 91×41 in the ξ and η directions, respectively, and the grids were non-uniformly and more closely spaced near the surface and in the wake of the cylinder. The skin friction, pressure, and Nusselt number distributions are the most sensitive quantities to be evaluated and are summarized in Table 1.

4. RESULTS AND DISCUSSION

4.1. *Non-dimensional parameters*

The non-dimensional parameters are the distance between the nozzle exit and the center of the cylinder H/R, the half width of the jet W/R, the non-dimensional wall temperature $\Delta = (T_w - T_a)/(T_j - T_a)$, Reynolds number Re, Grashof number Gr, and Prandtl number Pr. The magnitude of Gr/Re^2 indicates the importance of the effects of buoyancy with respect to forced convection. The length is non-dimensionalized by the radius of the cylinder R, velocity components by the jet velocity U_j, and temperature by $T_j - T_a$. The values of the non-dimensional parameters in the present numerical study were chosen by considering the OVD process and are given by:

$$Re = 100, 200, 300, 500, 700, 1000$$
$$Gr/Re^2 = 0.0, 0.1, 0.5, 1.0$$
$$H/R = 5.0, 10.0$$
$$W/R = 0.6, 0.8, 1.0.$$

For a cylinder radius of 0.01 m, a maximum air velocity of 2 m s^{-1}, and a maximum temperature difference between the jet and the cylinder of 2000 K, Re is less than 1000 and Gr is of the order of 10^6. The range of Reynolds numbers chosen covers the range where the jet is considerably diffused before reaching the stagnation point of the cylinder. The Prandtl number is fixed at 0.70. The jet is located on the center plane below the cylinder, and the vertical component of velocity and the temperature are assumed to be uniformly distributed at the nozzle exit.

The inlet boundary coincides with the exit plane of the nozzle and the downstream boundary is located at $x/R = 20.0$. The lateral boundaries are positioned at $y/R = \pm 15.0$. The domain is non-uniformly divided into 91×41 meshes. The grid points are carefully

Table 1

	Max. $C_f\sqrt{Re}$	Location
Experiment by Acrivos *et al.* [19]	2.62	50°
Calculation by Schuh [14]	2.49	50°
Present calculation	2.53	53.6°
	Min. C_p	Location
Experiment by Grove *et al.* [20]	−1.15	85°
Calculation by Schuh [14]	−1.22	90°
Present calculation	−1.08	91°
	Max. recirculation velocity (u/U_0)	Separation length (L_S/R)
Experiment by Coutanceau and Bouard [21]	−0.11	3.9
Calculation by Schuh [14]	−0.10	4.3
Present calculation	−0.11	4.1
	Average Nusselt number	
Exp. correlation by Collis and Williams [22]	1.58	
Exp. correlation by Hatton *et al.* [23]	1.65	
Calculation by Badr [24]	1.75	
Present calculation	1.64	

aligned near the cylinder surface to accurately determine the wall jet. Over the range of the non-dimensional parameters, the flow is symmetric. This has been calculated and was not assumed. Some solutions converge with oscillations at the downstream location, especially at the higher Reynolds numbers. The oscillations are small and do not significantly affect the skin-friction and heat transfer on the cylinder wall. The numerical results are considered to be converged when the largest non-dimensionalized residual of the variables is less than 1.0×10^{-4}. The relative variation in the maximum skin-friction coefficient, stagnation Nusselt number, and the averaged Nusselt number is less than 0.1% at each iteration with this criterion.

4.2. *Flow patterns and heat transfer*

The flow pattern around a cylinder without buoyancy is shown in Fig. 3 for $H/R = 10.0$, $W/R = 0.6$ and $Re = 100$. The flow regions noted in the Introduction are clearly present and entrained flow is observed. A large separation bubble is shown. The flow separates at $\theta = 96°$ and has a separation length $L_S/R = 7.4$ (measured from the rear of the cylinder; i.e. $L_S/R = 0.0$ when $x/R = 1.0$). As the Grashof number increases, the increased buoyancy accelerates the flow further downstream and the bubble size is considerably reduced (cf. Fig. 4, $L_S/R = 1.0$ for $Gr/Re^2 = 1.0$). In both cases the non-dimensional wall temperature of the cylinder is 0.5; for the case $Gr/Re^2 = 1.0$, isothermal contours are plotted in Fig. 5. The development of the flow and the temperature in the stagnation, boundary layer, separation, and recirculation regions are clearly shown. For large buoyancy the lateral extent of the wall jet flow and the heating effects are decreased due to the increased acceleration.

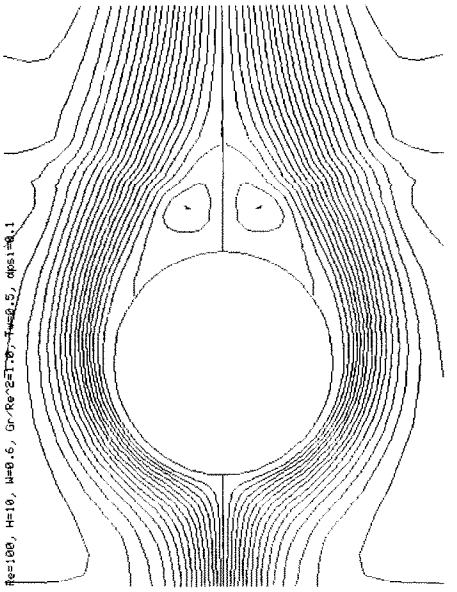

FIG. 4. Calculated streamline pattern with buoyancy; $H/R = 10.0$, $W/R = 0.6$, $Re = 100$, $Gr/Re^2 = 1.0$, $\Delta = 0.5$.

The variation of the skin friction and pressure coefficient are shown in Figs. 6 and 7, respectively for $Re = 100$, $\Delta = 0.5$, and for different values of Gr/Re^2. The results are symmetric about $\theta = 0$ (although the calculation was carried out over the entire domain $-180° < \theta < 180°$) and therefore only $0 < \theta < 180°$ are shown. The skin-friction increases from zero at the stagnation point to maximum values in the wall jet region, and then decreases to zero and negative values in the separated region. In the absence of buoyancy, the pressure coefficient has a maximum value of 1.0 at the stagnation point; larger values are obtained

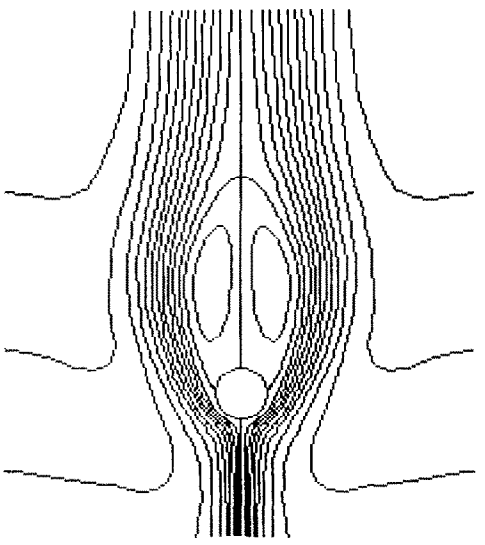

FIG. 3. Calculated streamline pattern in the absence of buoyancy; $H/R = 10.0$, $W/R = 0.6$, $Re = 100$, $Gr/Re^2 = 0.0$, $\Delta = 0.5$.

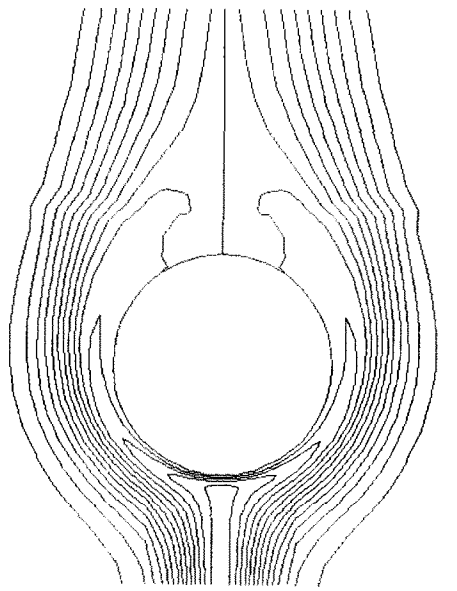

FIG. 5. Calculated temperature contours with buoyancy; $H/R = 10.0$, $W/R = 0.6$, $Re = 100$, $Gr/Re^2 = 1.0$, $\Delta = 0.5$.

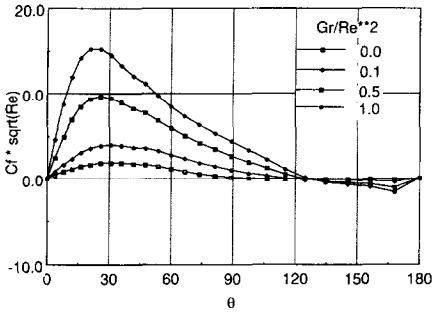

FIG. 6. Variation of skin-friction coefficient over the cylinder with buoyancy; $H/R = 10.0$, $W/R = 0.6$, $Re = 100$, $\Delta = 0.5$.

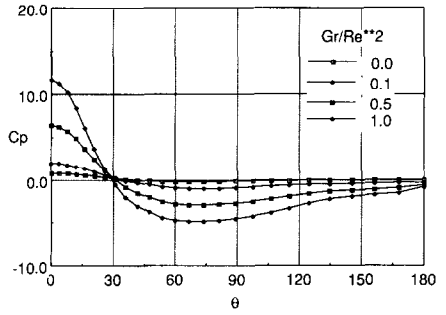

FIG. 7. Variation of pressure coefficient over the cylinder with buoyancy; $H/R = 10.0$, $W/R = 0.6$, $Re = 100$, $\Delta = 0.5$.

for increasing Gr/Re^2. The increase of the pressure coefficients corresponds to the increased acceleration of the impinging jet around the cylinder. The variation of the velocity along the center line is shown in Fig. 8. The velocity first increases and then decreases to zero at the stagnation point. When buoyancy is strong, the size of the recirculation region is reduced and the flow accelerates in the wake region downstream. The variation of the Nusselt numbers scaled by the square root of the Reynolds number and the temperature distribution along the center plane are shown in Figs. 9 and 10, respectively. The Nusselt number is a maximum at the stagnation point and this value increases with increasing Gr/Re^2. The stagnation Nusselt number, $Nu_0/\sqrt{Re}$ is 0.21 when $Gr/Re^2 = 0.0$ (cf. Fig. 9); note that the uniform inlet flow result is 0.34 as calculated by Mucoglu and Chen [25]. Their boundary layer calculations show a gradual reduction in the circumferential variation of the Nusselt number with some uncertainty near the separation point. The results in Fig. 9 (for the impinging jet) show a much more rapid decrease. The jet cools in the developing region and undergoes a sharp decrease to the wall temperature at the stagnation point. It is noted that it is difficult to predict the heat transfer with an impinging jet from the results that exist for uniform flow. In mixed convection heat transfer in uniform flow, buoyancy effects are limited to the boundary layer; however, for a jet they are dominant in the developing region ahead of the cylinder rather than in the wall jet region. The temperature near the rear stagnation point is increased by the hotter recirculating air from the surroundings; however, the jet cools gradually downstream. The general flow and temperature distributions are essentially unaltered when the Reynolds number increases; however, for large Reynolds number the jet accelerates with only a relatively weak viscous effect and cools less before reaching the cylinder. This results in higher skin-friction coefficients and Nusselt numbers.

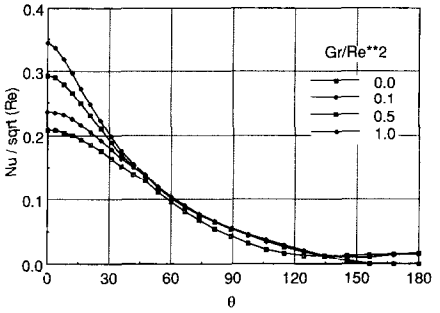

FIG. 9. Variation of Nusselt number over the cylinder with buoyancy; $H/R = 10.0$, $W/R = 0.6$, $Re = 100$, $\Delta = 0.5$.

For the non-dimensional cylinder wall temperature case of $\Delta = 0.5$, the air temperature near the wall is still higher than the wall temperature. The maximum temperature in the profile occurs away from the cylinder surface throughout the wall jet and recirculating regions. If the wall temperature is the same as the inlet jet temperature, i.e. $\Delta = 1.0$, the temperature of the jet will be less than the wall temperature, except in the limited region near the stagnation point. Therefore the jet does not heat the cylinder for this case. Cal-

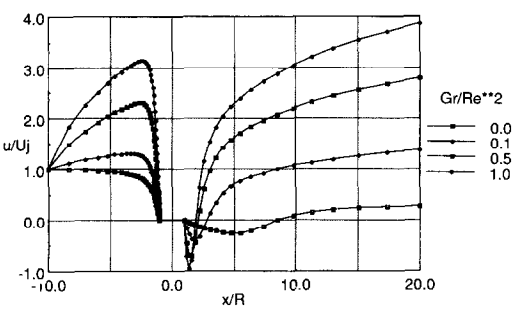

FIG. 8. Variation of velocity along the centerline with buoyancy; $H/R = 10.0$, $W/R = 0.6$, $Re = 100$, $\Delta = 0.5$.

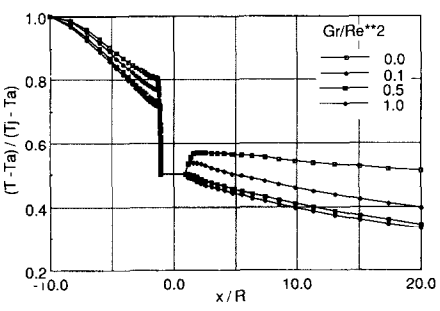

FIG. 10. Variation of temperature along the centerline with buoyancy; $H/R = 10.0$, $W/R = 0.6$, $Re = 100$, $\Delta = 0.5$.

culations were carried out for five dimensionless wall temperatures over the range from 0.5 to 1.0. The skin-friction coefficient and the velocity distribution along the center line are presented in Figs. 11 and 12, for $Re = 100$ and $Gr/Re^2 = 1.0$. The flow approaching the cylinder remains unchanged with respect to wall temperature; however, the flow downstream accelerates more rapidly with higher temperature and buoyancy as shown for $\Delta = 1.0$. The overall flow pattern is unchanged, with the separation point delayed (Fig. 11) and the separation length shortened (Fig. 12); i.e. there is a smaller recirculation region. The Nusselt number and temperature distributions are shown in Figs. 13 and 14. The local Nusselt number distributions change markedly with the wall tem-

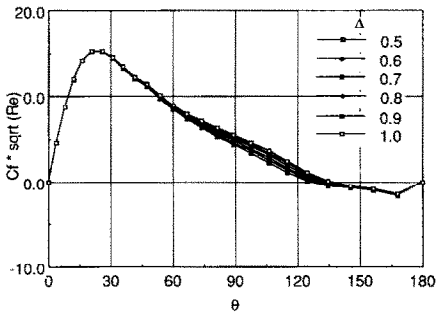

FIG. 11. Variation of skin-friction coefficient over the cylinder with wall temperature; $H/R = 10.0$, $W/R = 0.6$, $Re = 100$, $Gr/Re^2 = 1.0$.

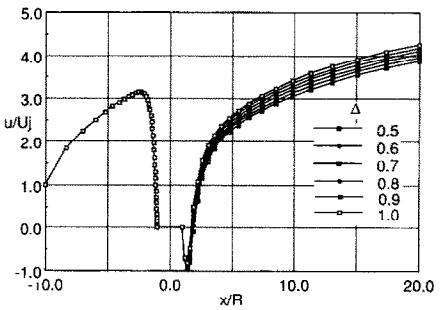

FIG. 12. Variation of velocity along the centerline with wall temperature; $H/R = 10.0$, $W/R = 0.6$, $Re = 100$, $Gr/Re^2 = 1.0$.

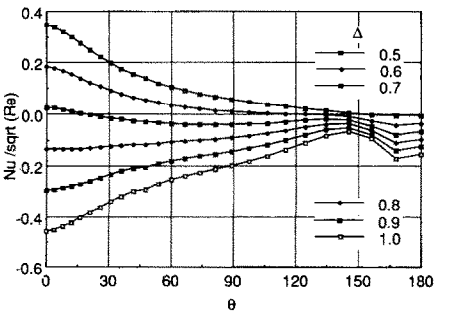

FIG. 13. Variation of Nusselt number over the cylinder with wall temperature; $H/R = 10.0$, $W/R = 0.6$, $Re = 100$, $Gr/Re^2 = 1.0$.

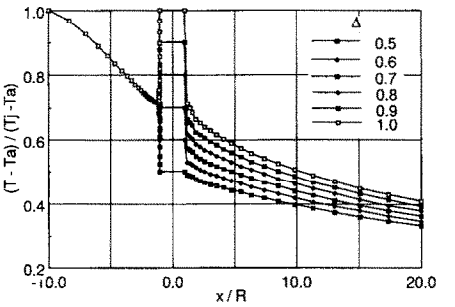

FIG. 14. Variation of temperature along the centerline with wall temperature; $H/R = 10.0$, $W/R = 0.6$, $Re = 100$, $Gr/Re^2 = 1.0$.

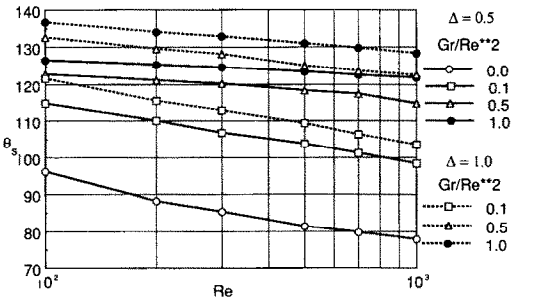

FIG. 15. Variation of separation point with Reynolds number, wall temperature and buoyancy; $H/R = 10.0$, $W/R = 0.6$.

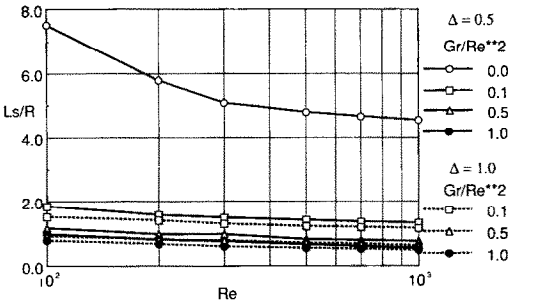

FIG. 16. Variation of separation length with Reynolds number, wall temperature and buoyancy; $H/R = 10.0$, $W/R = 0.6$.

perature and are almost proportional to the change of the wall temperature (Fig. 13).

The variation of the separation points and the separation lengths are presented in Figs. 15 and 16. The separation point moves downstream for smaller Reynolds number, higher wall temperature, and greater buoyancy. The separation lengths decrease for larger Reynolds number, higher wall temperature, and greater buoyancy.

The average Nusselt numbers are strongly dependent on the Reynolds and Grashof numbers, and the wall temperature. The acceleration of the jet ahead of the cylinder due to buoyancy is important and the average Nusselt number has been correlated using an effective Reynolds number. The effective Reynolds number includes a flow acceleration effect before the

stagnation point is reached. If the velocity and the temperature in the jet are constant up to a certain position ahead of the cylinder, the viscosity and conductivity can then be neglected in this region and the flow will be accelerated by buoyancy up to that location. An effective Reynolds number based on the accelerated velocity, which is determined from the Bernoulli equation, is given by

$$\frac{Re_{\text{eff}}}{Re} = \left\{1.0 + 2.0\frac{x_{\text{eff}}}{R}\frac{Gr}{Re^2}\right\}^{1/2}. \tag{11}$$

The effective distance x_{eff} is the distance from the nozzle to the location of the maximum velocity; for simplicity, we take $x_{\text{eff}} = H$, but a true effective distance would depend on the parameters. When the averaged Nusselt numbers are divided by the square root of the effective Reynolds numbers, considerably narrow banded curves are obtained for a given wall temperature, as is shown in Fig. 17 for $\Delta = 0.5$ and $\Delta = 1.0$. The Nusselt numbers for wall temperatures between $\Delta = 0.5$ and 1.0 can be estimated by linear interpolation.

4.3. *Effects of the width of the jet and the distance between the nozzle and the cylinder*

The flow and heat transfer are dependent on the width of the jet. As the width of the jet becomes larger, the effects of viscous diffusion and heat loss from the jet are reduced, and the maximum velocity and the jet temperature increase with increasing W/R (cf. Fig. 18 for the temperature profile for $W/R = 1.0$, 0.8 and 0.6

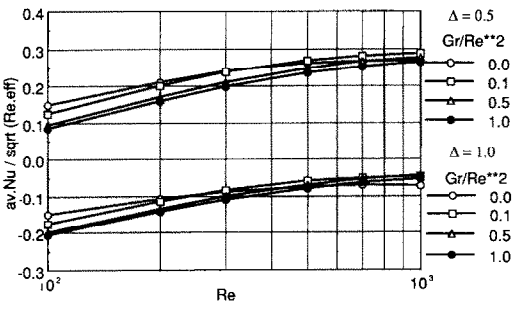

FIG. 17. Scaled average Nusselt numbers; $H/R = 10.0$, $W/R = 0.6$.

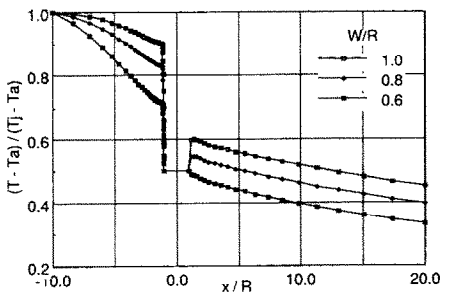

FIG. 18. Variation of temperature along the centerline with jet width; $H/R = 10.0$, $Re = 100$, $Gr/Re^2 = 1.0$, $\Delta = 0.5$.

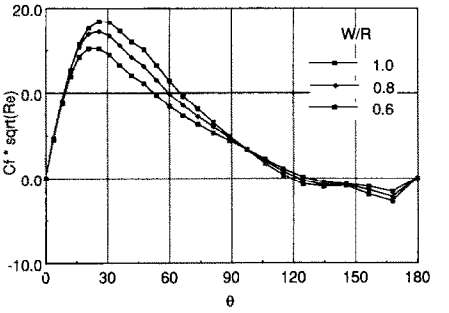

FIG. 19. Variation of skin-friction coefficient over the cylinder with jet width; $H/R = 10.0$, $Re = 100$, $Gr/Re^2 = 1.0$, $\Delta = 0.5$.

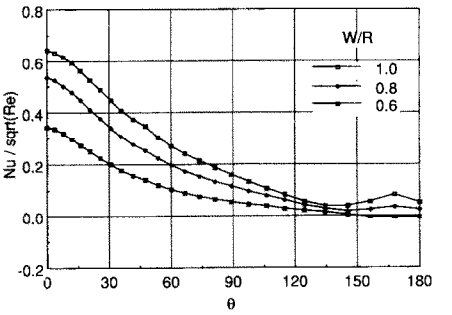

FIG. 20. Variation of Nusselt number over the cylinder with jet width; $H/R = 10.0$, $Re = 100$, $Gr/Re^2 = 1.0$, $\Delta = 0.5$.

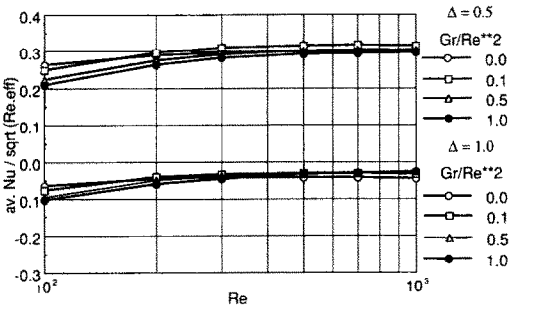

FIG. 21. Scaled average Nusselt numbers; $H/R = 10.0$, $W/R = 1.0$.

for H/R fixed at 10.0). These effects result in higher skin-friction and Nusselt numbers, as shown in Figs. 19 and 20. At the higher Reynolds numbers, the changes in the scaled skin-friction and Nusselt number are not large; however, the flow and the temperature distributions in the wall jet and in the recirculation region are changed considerably. The thicker jet width, $W/R = 1.0$, results in a larger recirculation bubble due to the earlier separation of the flow, and the scaled Nusselt numbers show higher values (Fig. 21) than were obtained for the case $W/R = 0.6$ (Fig. 17).

The distance between the nozzle and the cylinder, H, also has a considerable effect on the flow and heat transfer. Calculations have been carried out for $H/R = 5.0$ and $W/R = 0.6$. The results are compared with those for $H/R = 10.0$ and $W/R = 0.6$, which

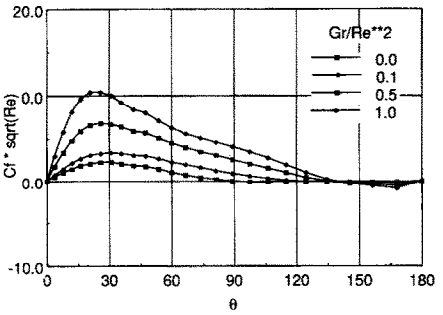

FIG. 22. Variation of skin-friction coefficient over the cylinder with buoyancy; $H/R = 10.0$, $W/R = 0.6$, $Re = 100$, $\Delta = 0.5$.

were discussed previously. For the short distance $H/R = 5.0$, the time for flow-acceleration as well as for viscous diffusion is reduced. The maximum velocities are not as large as those for the longer distance, and also the heat losses become smaller. Furthermore, when the cylinder is placed closer to the nozzle, the increased blockage shifts the wall jet profile to the outside. The reduction in the impinging velocity reduces the maximum values of the skin-friction (Fig. 22). However, the heat transfer is increased, especially near the stagnation point (Fig. 23), which corresponds to the reduced heat losses in the developing jet region. At the higher Reynolds numbers, the effects of the reduced flow-acceleration for the shorter distance H are dominant and both the stagnation and averaged Nusselt numbers become smaller for smaller H. The averaged Nusselt numbers scaled by the effective Reynolds number are presented in Fig. 24.

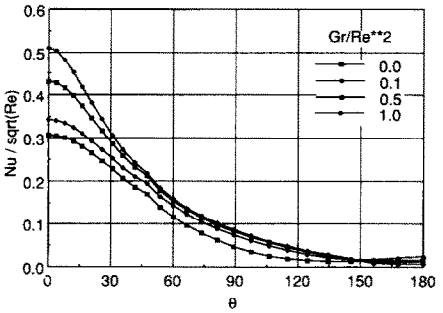

FIG. 23. Variation of Nusselt number over the cylinder with buoyancy; $H/R = 10.0$, $W/R = 0.6$, $Re = 100$, $\Delta = 0.5$.

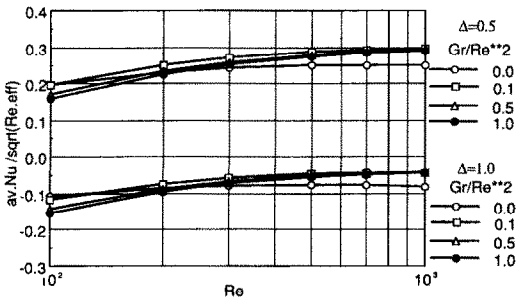

FIG. 24. Scaled average Nusselt numbers; $H/R = 5.0$, $W/R = 0.6$.

5. CONCLUSIONS

Numerical solutions have been obtained for the flow and heat transfer resulting from the impingement of a plane laminar hot air jet on a circular cylinder. The effects of the Reynolds and Grashof numbers as well as those of the wall temperature, the jet width, and the distance between the nozzle and the cylinder have been investigated. The following conclusions are drawn.

(1) The flow is stable and symmetric over the range of the parameters studied. The interaction of the buoyant impinging jet with the cylinder results in flow and heat transfer that are quite different from that for uniform flow.

(2) The effect of buoyancy accelerates the jet ahead of the cylinder and reduces the separation bubble downstream of the cylinder. This results in an increase in the Nusselt number.

(3) The diffusion and cooling of the hot impinging jet at low Reynolds numbers are less than those occurring at high Reynolds numbers. The average Nusselt number increases with increasing Reynolds number.

(4) The wall temperature does not significantly affect the flow over the cylinder so that the average Nusselt number decreases linearly with the wall temperature. The average heat transfer becomes zero for a wall temperature that is less than that of the hot jet.

(5) The average Nusselt number increases with Reynolds number and Grashof number. Narrow banded correlation curves are obtained by introducing an effective Reynolds number.

(6) Viscous diffusion and heat loss from the jet to the surroundings are reduced in a wide jet. These effects result in higher skin-friction and Nusselt numbers.

(7) As the distance between the nozzle and the cylinder decreases, both the stagnation and the average Nusselt numbers increase at low Reynolds numbers. The effect of reduced flow-acceleration is dominant at the higher Reynolds numbers and results in smaller values for the heat transfer.

Acknowledgements—Support from the National Science Foundation, the San Diego Supercomputer Center and the Computer Center of the University of California at Berkeley is gratefully acknowledged. The authors are indebted to Professor J. A. C. Humphrey for the use of his numerical code for non-orthogonal coordinates.

REFERENCES

1. G. M. Homsy, F. T. Geyling and K. L. Walker, Blasius series for thermophoretic deposition of small particles, *J. Colloid Interface Sci.* **83**, 495–501 (1981).
2. G. K. Batchelor and C. Shen, Thermophoretic deposition of particles in gas flowing over cold surfaces, *J. Colloid Interface Sci.* **107**, 21–37 (1985).
3. V. K. Garg and S. Jayaraj, Thermophoretic deposition over a cylinder, *Int. J. Engng Fluid Mech.* **3**, 175–196 (1990).
4. V. K. Garg and S. Jayaraj, Thermophoretic deposition

in crossflow over a cylinder, *J. Thermophys.* **4,** 115–116 (1990).
5. M. K. Alam, G. Graham, V. Janakiraman and J. Greaves, Numerical analysis of thermophoretic transport in the OVD process, *Numer. Heat Transfer, ASME HTD* **130,** 67–72 (1990).
6. J. R. Bautista, K. L. Walker and R. M. Atkins, Modeling of heat transfer and mass transfer in the manufacture of optical waveguides, A.I.Ch.E. National Meeting at Washington, DC (1988).
7. G. M. Graham and M. K. Alam, Experimental study of the outside vapor deposition process (in preparation, 1992).
8. A. Zukauskas, Heat transfer from tubes in crossflow, *Adv. Heat Transfer* **8,** 93–159 (1972).
9. V. T. Morgan, The overall convective heat transfer from smooth circular cylinders, *Adv. Heat Transfer* **11,** 199–264 (1975).
10. B. Gebhart, Y. Jaruria, R. L. Mahajan and B. Sammakia, *Buoyancy-induced Flows and Transport.* Springer-Verlag, Berlin (1988).
11. J. M. F. Vickers, Heat transfer coefficients between fluid jets and normal surfaces, *Ind. Engng Chem.* **51,** 967–972 (1959).
12. E. Gutmark, M. Wolfstein and I. Wygnanski, The plane turbulent impinging jet, *J. Fluid Mech.* **88,** 737 756 (1978).
13. J. F. Thompson, Z. A. Warsi and C. W. Mastin, *Numerical Grid Generation, Foundations and Applications.* North-Holland, New York (1985).
14. M. J. Schuh, Numerical prediction of fluid and particle motions in flows past tubes, Ph.D. Thesis, University of California, Berkeley (1987).
15. M. J. Schuh, C. A. Schuler and J. A. C. Humphrey, Numerical calculation of particle-laden gas flows past tubes, *A.I.Ch.E. Jl* **35,** 466–480 (1989).
16. S. V. Patankar, *Numerical Heat Transfer and Fluid Flow.* Hemisphere, New York (1980).
17. G. E. Schneider and M. Zedan, A modified strongly implicit procedure for the numerical solution of field problems, *Numer. Heat Transfer* **4,** 1–19 (1981).
18. G. De Vahl Davis, Natural convection of air in a square cavity: a bench mark numerical solution, *Int. J. Numer. Meth. Fluids* **3,** 249–264 (1983).
19. A. Acrivos, L. G. Leal, D. D. Snowden and F. Pan, Further experiments on steady separated flows past bluff objects, *J. Fluid Mech.* **34,** Part 1, 25–48 (1968).
20. A. S. Grove, F. H. Shair, E. E. Petersen and A. Acrivos, An experimental investigation of the steady separated flow past a circular cylinder, *J. Fluid Mech.* **19,** 60–81 (1964).
21. M. Coutanceau and R. Bouard, Experimental determination of the main features of the viscous flow in the wake of a circular cylinder in uniform translation. Part 1. Steady flow, *J. Fluid Mech.* **79,** Part 2, 231–256 (1977).
22. D. C. Collis and M. J. Williams, Two-dimensional convection from heated wires at low Reynolds numbers, *J. Fluid Mech.* **6,** 357–384 (1959).
23. A. P. Hatton, D. D. James and H. W. Swire, Combined forced and natural convection with low speed air flow over horizontal cylinders, *J. Fluid Mech.* **42,** 17 31 (1970).
24. H. M. Badr, A theoretical study of laminar mixed convection from a horizontal cylinder in a cross stream, *Int. J. Heat Mass Transfer* **26,** 639–653 (1983).
25. A. Mucoglu and T. S. Chen, Analysis of combined forced and free convection across a horizontal cylinder, *Can. J. Chem. Engng* **55,** 265–270 (1977).

ECOULEMENT ET TRANSFERT THERMIQUE AUTOUR D'UN CYLINDRE CIRCULAIRE AVEC UN JET D'AIR CHAUD IMPACTANT

Résumé—On étudie l'écoulement et le transfert thermique d'un jet chaud d'air impactant un cylindre circulaire. L'intérêt du problème est fondamental à cause des applications importantes, en particulier au procédé de dépôt de vapeur. Des solutions numériques des équations de bilan sont obtenues en utilisant une grille de coordonnées curvilinéaires non orthogonales. On étudie les effets sur les nombres de Reynolds et de Grashof de la largeur du jet et de la distance entre la tuyère et le cylindre et des courbes sont présentées. L'écoulement est stable et symétrique pour le domaine des paramètres étudiés. L'interaction du flottement du jet impactant avec le cylindre aussi bien qu'avec l'environnement fait que l'écoulement et le transfert thermique sont complètement différents de ce qu'ils sont pour un écoulement uniforme. Les effets du flottement, de la diffusion et du refroidissement du jet devant le cylindre, le développement du jet pariétal et la bulle de recirculation affectent l'écoulement et le transfert thermique. La largeur du jet et la distance entre la tuyère et le cylindre ont une forte influence sur le transfert thermique.

STRÖMUNG UND WÄRMEÜBERGANG AN EINEM KREISZYLINDER MIT EINEM HEISSEN AUFTREFFENDEN LUFTSTRAHL

Zusammenfassung—In der vorliegenden Arbeit werden die Strömung und der Wärmeübergang an einem Kreiszylinder, auf den ein heißer Luftstrahl auftrifft, untersucht. Das Problem ist von grundlegendem Interesse und hat auch wichtige Anwendungen. Mit Hilfe eines nicht-orthogonalen gekrümmten Koordinatensystems wurden die grundlegenden Erhaltungsgleichungen numerisch gelöst. Die Einflüsse der Reynolds-Zahl und der Grashof-Zahl sowie der Wandtemperatur, der Strahlbreite und des Abstandes zwischen Düse und Zylinder auf Strömung und Wärmeübergang wurden untersucht und mittels Korrelationskurven dargestellt. Die Strömung ist über den Bereich der untersuchten Parameter stabil und symmetrisch. Die Wechselwirkung zwischen dem auftreffenden Auftriebsstrahl und dem Zylinder sowie der Umgebung unterscheidet Strömung und Wärmeübergang am Zylinder stark von den Vorgängen bei gleichförmiger Strömung. Die Auswirkungen von Auftrieb, Diffusion und Kühlung des Strahls vor dem Auftreffen auf den Zylinder, die Ausbildung des Wandstrahls und die rezirkulierende Blase beeinflussen Strömung und Wärmeübergang. Die mittlere Nusselt-Zahl wird mit zunehmenden Werten von Reynolds- und Grashof-Zahl größer. Durch Einführen einer effektiven Reynolds-Zahl mit einem Auftriebsterm erhält man eng begrenzte Korrelationskurven. Die Breite des Strahls und der Abstand zwischen Düse und Zylinder haben einen starken Einfluß auf den Wärmeübergang.

ТЕЧЕНИЕ И ТЕПЛОПЕРЕНОС К КРУГОВОМУ ЦИЛИНДРУ ПРИ ПАДЕНИИ НА НЕГО НАГРЕТОЙ СТРУИ ВОЗДУХА

Аннотация—Исследуются течение и теплоперенос к круговому цилидру от нагретой набегающей струи воздуха. Здача представляет научный интерес и имеет важные приложения, например, в процессах внешнего осаждения пара. С использованием сетки неортогональных криволинейных координат получены численные решения уравнений сохранения. Исследуется влияние чисел Рейнольдса и Грасгофа, а также температуры стенки, диаметра струи и расстояния между соплом и пилиндром на течение и теплоперенос, и приводятся соответствующие графики. В исследуемом диапазоне параметров течение является стационарным и симметричным. При взаимодействии плавучей струи с цилиндром и окружающей средой течение и теплоперенос существенно отличаются от случая вынужденного равномерного течения. На течение и теплоперенос оказывают влияние подъемная сила, охлаждение струи перед цилиндром, развитие пристенной струи и возвратного течения. Среднее число Нуссельта увеличивается с ростом чисел Рейнольдса и Грасгофа. С использованием эффективного числа Рейнольдса, учитывающего вклад подъемных сил, получены обобщающие зависимости. Диаметр струи и расстояние между соплом и цилиндром существенно влияют на теплоперенос.